

Contents

1 Theory	3
1.1 Sesquioxides	3
1.1.1 Chromium Oxide	4
1.1.2 Gallium Oxide	7
1.2 X-ray Diffraction Principles	8
1.2.1 Scattering at Lattices	8
1.2.2 X-rays	9
1.3 Heteroepitaxy	10
1.3.1 Pseudomorphic Growth	10
1.3.2 Relaxed Growth	11
Dislocations	11
Slip Systems for Sesquioxide Heterostructures	12
2 Experimental Methods	15
2.1 Pulsed Laser Deposition	15
2.1.1 Setup	15
2.1.2 Plasma Dynamics	17
2.1.3 Segmented Target Approach	17
2.2 X-Ray Diffraction Measurement	18
2.2.1 2θ - ω -scans	18
2.2.2 ω -scans	19
2.2.3 ϕ -scans	20
2.2.4 Reciprocal Space Maps	20
2.2.5 Technical Details	22
2.3 Thermal Evaporation	23
2.4 Resistivity Measurement	24
2.5 Thickness Determination	25
2.6 Spectral Transmission	26
2.7 Further Measurement Methods	27
3 Experiment, Results and Discussion	28
3.1 Preliminary Investigations	28
3.1.1 Experiment	28
3.1.2 Oxygen Partial Pressure Variation on <i>m</i> -plane Sapphire	28
3.1.3 Growth Temperature Variation on <i>m</i> -plane Sapphire	33
3.1.4 Influence of Growth Rate on Crystal Structure	33
3.1.5 Deposition on <i>c</i> -, <i>r</i> -, <i>m</i> - and <i>a</i> -plane Sapphire	35
3.1.6 Conclusion	37
3.2 Discrete Combinatorial Synthesis for Taylored Doping	39
3.2.1 Experiment	39

3.2.2	DCS with Different Targets	39
3.2.3	Conclusion	45
3.3	Strain Analysis	48
3.3.1	Experiment	49
3.3.2	Growth Rates	53
3.3.3	Strain and Tilt for Different Orientations	53
3.3.4	Conclusion	67
3.4	Cr ₂ O ₃ Buffer Layers for α -Ga ₂ O ₃	69
3.4.1	Experiment	69
3.4.2	Comparison of <i>in situ</i> and <i>ex situ</i> grown Ga ₂ O ₃ on Chromia Buffers	70
3.4.3	Conclusion	74
Appendices		76
A Calculations		77
A.1	<i>m</i> -plane lattice constants	77
A.2	<i>a</i> -plane lattice constants	77
B Figures		79
Bibliography		85

Chapter 3

Experiment, Results and Discussion

Contents

3.1 Preliminary Investigations	28
3.1.1 Experiment	28
3.1.2 Oxygen Partial Pressure Variation on <i>m</i> -plane Sapphire	28
3.1.3 Growth Temperature Variation on <i>m</i> -plane Sapphire	33
3.1.4 Influence of Growth Rate on Crystal Structure	33
3.1.5 Deposition on <i>c</i> -, <i>r</i> -, <i>m</i> - and <i>a</i> -plane Sapphire	35
3.1.6 Conclusion	37
3.2 Discrete Combinatorial Synthesis for Taylored Doping	39
3.2.1 Experiment	39
3.2.2 DCS with Different Targets	39
3.2.3 Conclusion	45
3.3 Strain Analysis	48
3.3.1 Experiment	49
3.3.2 Growth Rates	53
3.3.3 Strain and Tilt for Different Orientations	53
3.3.4 Conclusion	67
3.4 Cr₂O₃ Buffer Layers for α-Ga₂O₃	69
3.4.1 Experiment	69
3.4.2 Comparison of <i>in situ</i> and <i>ex situ</i> grown Ga ₂ O ₃ on Chromia Buffers	70
3.4.3 Conclusion	74

3.4 Cr₂O₃ Buffer Layers for α -Ga₂O₃

A major motivation for investigating Cr₂O₃ thin films is a possible usage as buffer layer for isostructural α -Ga₂O₃, which has similar lattice parameters: Cr₂O₃ has a slightly larger c and smaller a lattice constant than α -Ga₂O₃ (Fig. 3.37). This could improve the crystal quality of α -Ga₂O₃ thin films due to reduced lattice mismatch when compared to Al₂O₃ [1]. For c -plane, the mismatch of α -Ga₂O₃ to Al₂O₃ and Cr₂O₃ is 4.6 % and 0.4 %, respectively. However, as shown in chapter 3.3, the in-plane compressive strain for Cr₂O₃ thin films on c -plane Al₂O₃ increases the mismatch between Cr₂O₃ and α -Ga₂O₃ slightly for the pseudomorphic grown thin films. However, when supplying sufficiently thick samples of at least 150 nm, this strain is negligible. On the other side, for m -plane samples, the mismatch of α -Ga₂O₃ to Al₂O₃ and Cr₂O₃ regarding the c -axis is 3.3 % and -1.2 %, respectively. Furthermore, as shown in the previous chapter, the in-plane compressive strain for m -plane Cr₂O₃ thin films yields less discrepancy between the c lattice constant of both sesquioxides. A similar argument can be drawn for a -plane samples. In the following, a proof of concept will be given that α -Ga₂O₃ can be successfully deposited on Cr₂O₃ buffer layers.

3.4.1 Experiment

For the Cr₂O₃ thin films, deposition parameters were chosen that yield the lowest strain and smallest ω -FWHM. Therefore, a lens position of -1 cm and a laser pulse energy of 450 mJ were applied. Note that 350 mJ would result in even less strain, but only at the cost of very low growth rates and less crystallinity. The Ga₂O₃ layer was deposited with a lens position of -2 cm and a laser pulse energy of 650 mJ, being known as optimal for α -Ga₂O₃ deposition in this chamber. This is the configuration that was used for depositing Cr₂O₃ in 3.1 and 3.2. By assuming a growth rate of 10 pm pulse⁻¹ – which is achieved for deposition with similar parameters at a different PLD chamber –, 15 000 pulses were applied to achieve a layer thickness of approx. 150 nm. The oxygen partial pressure was 3×10^{-4} mbar and the temperature was chosen to be approx. ???. Two approaches were chosen to deposit α -Ga₂O₃ of four different orientations c , r , m and a :

1. Deposition of Cr₂O₃ with subsequent *ex situ* analysis of the Cr₂O₃ layer under atmospheric conditions. Afterwards the Ga₂O₃ layer was deposited in an additional PLD process.

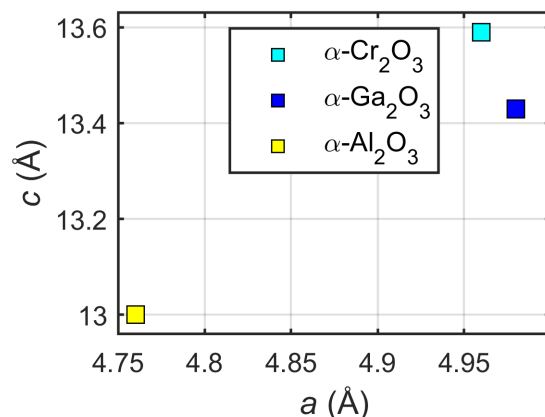


Figure 3.37: Lattice constants a and c for the three sesquioxides relevant in this work.

2. *In situ* deposition of Cr₂O₃ and Ga₂O₃ without returning to atmospheric conditions inbetween. Between both processes, the oxygen pressure was reduced and it was waited for 20 min to achieve thermodynamic equilibrium.

For the *ex situ* samples, Reciprocal Space Maps (RSMs) around the exptected α -phase symmetric reflection were recorded before and after the deposition of the Ga₂O₃ layer to confirm the formation of the α -phase. Furthermore, 2 θ - ω -scans were performed for all samples after deposition of the Ga₂O₃ layer to check whether other phases are present. To confirm the crystallinity of the Ga₂O₃ layer, Reflection High-Energy Electron Diffraction (RHEED) patterns were recorded for the surfaces of all samples after deposition of the Ga₂O₃ layer.

The 2 θ - ω patterns are compared to a reference Cr₂O₃ sample from chapter 3.3, fabricated with a pulse energy of 450 mJ. The theoretical predictions of the 2 θ values for reflections of β -Ga₂O₃ were taken from the *Materials Project* [2, mp-886].

Transmission Electron Microscopy (TEM) and Energy-dispersive X-Ray Spectroscopy (EDX) measurements were performed by Dr. J. G. Fernandez from *Centre for Materials Science and Nanotechnology Physics*, Oslo, and kindly provided the images, shown in Figs. 3.40, 3.41 and 3.42.

3.4.2 Comparison of *in situ* and *ex situ* grown Ga₂O₃ on Chromia Buffers

The RHEED patterns of all samples from the *ex situ* and the *in situ* batch are depicted in Fig. 3.38a and Fig. 3.38b, respectively. From the periodic patterns it can be concluded that every surface is crystalline. Note that the mere observation of crystallinity does not indicate which phase of Ga₂O₃ is present on the samples.

c-plane α -Ga₂O₃ grown on Cr₂O₃

To determine the present crystal phases of the Ga₂O₃ thin film, in Fig. 3.39a, 2 θ - ω patterns of the samples deposited on *c*-plane Al₂O₃ are depicted, namely the Cr₂O₃ reference sample (black), as well as the *ex situ* (blue) and *in situ* (red) samples. The peak at around 39.2° of the refefence sample is the (00.6) reflection of Cr₂O₃. This reflection is also attributed to the peaks at approx. 39.4° and 39.6° of the *ex situ* and *in situ* samples, respectively. The variation of peak position for the Cr₂O₃ layer may originate in the fact that for each process, the thickness may have varied. As discussed in chapter 3.3, this is a crucial factor for the out-of-plane strain and therefore the position of the reflection. In addition, two overlaying peaks occur at 40.14° for both buffer layer processes. This is attributed to the (00.6) reflection of α -Ga₂O₃, because the predicted peak position is at 40.26° with a relative intensity of 3.37, and is therefore allowed. The presence of two peaks is attributed to the splitting between Cu-K α_1 and Cu-K α_2 radiation (*Ka splitting*). Note that at approx. 86°, the higher order (00.12) reflection of Cr₂O₃ can be observed more dominantly than the (00.12) reflection of α -Ga₂O₃. This is due to the fact the the ratio of relative intensities of (00.12) to (00.6) is 29.6 % for Cr₂O₃ and only 1.4 % for α -Ga₂O₃.

For the *in situ* sample, no additional peaks are observed, indicating phase-pure deposition of *c*-plane Ga₂O₃ in the α -phase on *c*-plane Al₂O₃. For the *ex situ* sample, however, a peak occurs at 38.78° and both the β - and κ -phase of Ga₂O₃ have a predicted peak at this position, listed in Tab. 3.5. The observed peak is attributed to the (004) reflection of the κ -phase. A lower order of this reflection is also observed at 19.13°, which is attributed to the (002) reflection of κ -Ga₂O₃. Note that the peak observed at

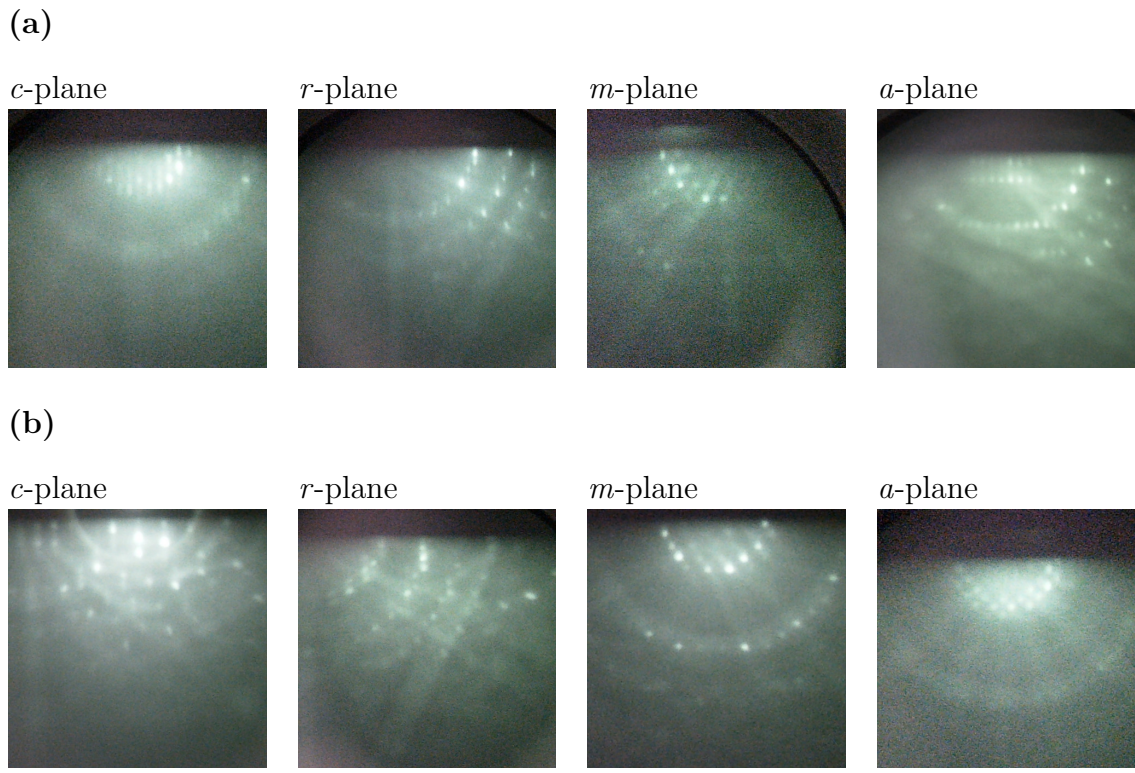


Figure 3.38: RHEED patterns of the α -Ga₂O₃ surface deposited (a) *ex situ* on Cr₂O₃ and (b) *in situ* on Cr₂O₃. Note that the patterns were recorded in arbitrary azimuth which is why they may differ between *ex situ* and *in situ* deposition. This is not necessarily a result of different crystal structure.

20.4° is also observed for the Cr₂O₃ reference sample and can therefore not correspond to any Ga₂O₃ phase. It can be concluded that the *ex situ* growth of Ga₂O₃ on a *c*-plane Cr₂O₃ buffer layer results in both α -Ga₂O₃ and χ -Ga₂O₃, with the latter being much less pronounced.

In Fig. 3.39b, the RSMs of the *ex situ* *c*-plane sample are displayed before and after deposition of Ga₂O₃. Note that the image is cropped such that no substrate peak is visible. The previous result is confirmed that another phase has formed on top of the Cr₂O₃ layer. No ω -scans were done, but the crystallinity can be estimated by the broadening in q_{\parallel} direction, which is less dominant in comparison to the Cr₂O₃ layer. Furthermore, the K α splitting indicates a highly crystalline thin film.

In Fig. 3.40, HAADF images are shown for the interface between α -Ga₂O₃ and Cr₂O₃. The *c*-axis points upwards, and the atom arrangement that is visible corresponds to the *a*-plane. The similar crystal structure can be clearly seen by comparing

Table 3.5: Selected reflections of β -Ga₂O₃ [2, mp-886] and χ -Ga₂O₃ [3] and their predicted positions in 2θ - ω patterns, as well as the observed peak position for Ga₂O₃ deposited *ex situ* on Cr₂O₃ (blue curve in Fig. 3.39a).

Phase	2θ	reflection	measured
β -Ga ₂ O ₃	18.89°	(20 $\bar{1}$)	19.13°
χ -Ga ₂ O ₃	19.11°	(002)	
β -Ga ₂ O ₃	38.32°	(40 $\bar{2}$)	38.78°
χ -Ga ₂ O ₃	38.77°	(004)	

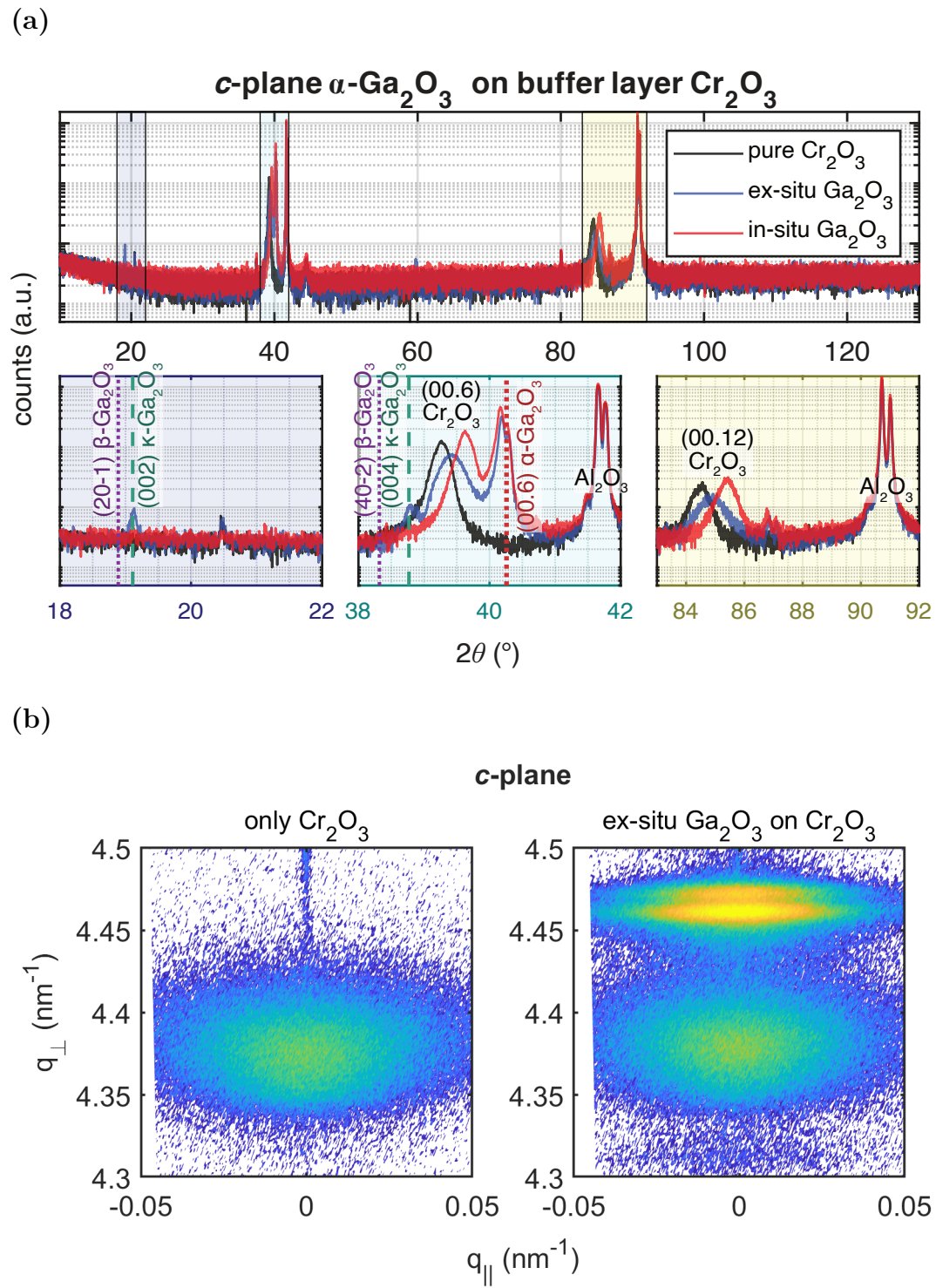


Figure 3.39: (a) $2\theta\text{-}\omega$ -patterns of the c -plane Cr_2O_3 reference sample (black), as well as the *ex situ* (blue) and *in situ* (red) buffer layer structures. The expected peak positions of $\beta\text{-Ga}_2\text{O}_3$ (purple dotted) and $\kappa\text{-Ga}_2\text{O}_3$ (green dashed) from Tab. 3.5 are indicated, as well as the (00.6) reflection of $\alpha\text{-Ga}_2\text{O}_3$ (red dotted). (b) RSM around the (00.6) reflection recorded before (left) and after (right) *ex situ* deposition of Ga_2O_3 on Cr_2O_3 .

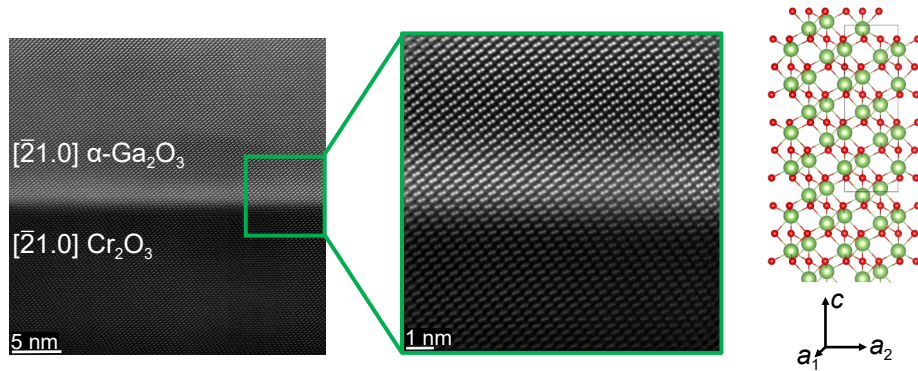


Figure 3.40: HAADF image of the interface between *c*-plane Cr_2O_3 and $\alpha\text{-}\text{Ga}_2\text{O}_3$. The $[2\bar{1}.0]$ direction points into the plane of the paper, i.e. the *a*-plane is visible. Courtesy of Dr. J. G. Fernandez. The image of the $\alpha\text{-}\text{Ga}_2\text{O}_3$ crystal structure was made with VESTA Ver. 3 [4].

the lattice spacing of the upper and lower half plane. No dislocations form at the interface and the (00.1)-orientation of the Cr_2O_3 buffer continues for the Ga_2O_3 layer.

m-, *a*- and *r*-plane $\alpha\text{-}\text{Ga}_2\text{O}_3$ grown on Cr_2O_3

When comparing the peaks of *m*-plane buffer layer samples to the Cr_2O_3 reference sample, note that the (30.0) peak is shifted to lower angles (Fig. 3.43a), i.e. that the buffer layers are more strained when compared to the reference sample. Note that for the buffer layers, a new Cr_2O_3 target has been used. This could be the reason for the increased strain as shown in chapter 3.2, where target degradation reduced the peak shift in $2\theta\text{-}\omega$ patterns. Furthermore, two peaks can be observed for the buffer layer samples, which may originate in (i) either two peaks for Cr_2O_3 and $\alpha\text{-}\text{Ga}_2\text{O}_3$ each; or (ii) $\text{K}\alpha$ splitting of a (30.0) $\alpha\text{-}\text{Ga}_2\text{O}_3$ reflection on top of the Cr_2O_3 layer. Both explanations are favored by the fact that the expected peak position (red dotted line) lays inbetween both peaks. The theoretical predictions of the 2θ positions also have similar distance as the two peaks observed (red and green dotted lines), favoring the first explanation. However, when considering Fig. 3.43b, it becomes clear that the origin is a $\text{K}\alpha$ splitting, because prior to the deposition of Ga_2O_3 , none of the peaks was present with the observed intensity. Therefore, the observed peaks must both stem from the α -phase of Ga_2O_3 . No other peaks are observed in the $2\theta\text{-}\omega$ pattern, therefore only the α -phase is present.

In Fig. 3.41a, an HAADF image of the *m*-plane buffer layer structure is depicted. The [10.0] direction points upwards, and the atom arrangement that is visible corresponds to the *c*-plane. In the $\alpha\text{-}\text{Ga}_2\text{O}_3$ layer, threading dislocations can be seen. The expected composition of the layers is confirmed by spatially resolved EDX measurements (cf. Fig. 3.41b). A detailed view into the interface between Cr_2O_3 and $\alpha\text{-}\text{Ga}_2\text{O}_3$ is given in Fig. 3.42a. Similar to the *c*-plane structure, the (10.0) orientation of the buffer layer is continued in the $\alpha\text{-}\text{Ga}_2\text{O}_3$ layer, which exhibits very good crystal quality, as can be seen in Fig. 3.42b.

A similar behavior as for the *m*-plane samples can be observed in the $2\theta\text{-}\omega$ patterns of *a*-plane samples (Fig. 3.44a). The splitted peak is attributed to the (22.0) reflection of an $\alpha\text{-}\text{Ga}_2\text{O}_3$ layer and the peak on the left shoulder to the (22.0) reflection of Cr_2O_3 , which is shifted to lower angles in comparison to the reference sample. This behavior is also observed for the (11.0) reflections of both $\alpha\text{-}\text{Ga}_2\text{O}_3$ and Cr_2O_3 . This result is confirmed by the RSMs (Fig. 3.44b), where two peaks appear due to $\text{K}\alpha$ splitting

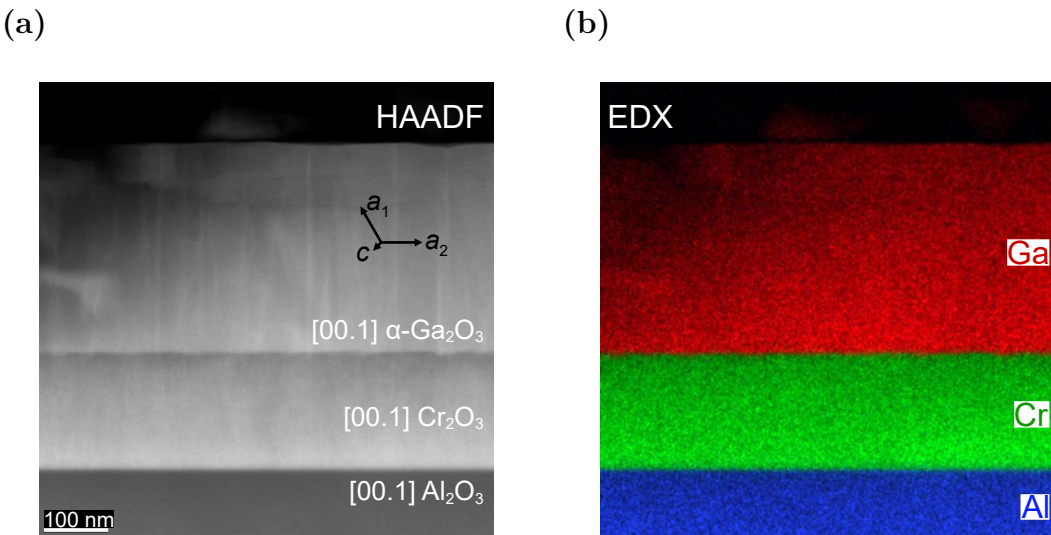


Figure 3.41: Images of the m -plane buffer layer structure: (a) HAADF image and (b) spatially resolved EDX data of the Al₂O₃, Cr₂O₃ and α -Ga₂O₃ layer. The c -axis points into the plane of the paper. Courtesy of Dr. J. G. Fernandez.

after Ga₂O₃ deposition. The low broadening in q_{\parallel} direction as well as the K α splitting indicate good crystal quality.

The $2\theta-\omega$ patterns of the r -plane reference and buffer layer samples are depicted in Fig. 3.45a. Due to very close peak positions of the (02.4) reflection for both Cr₂O₃ and α -Ga₂O₃, a comparison with the reference sample (black) is not as straightforward as for the other orientations. No additional peak can be identified for the buffer layer samples. However, the RHEED patterns indicated a crystalline surface, which is why the only possible phase of the Ga₂O₃ layer is the α -phase. This is verified by RSMs of the *ex situ* sample in Fig. 3.45b: a significant increment in intensity can be observed at the expected peak position of (02.4) α -Ga₂O₃, which is due to the formation of α -phase Ga₂O₃ on r -plane Cr₂O₃.

3.4.3 Conclusion

Phase-pure depositon of α -Ga₂O₃ on Cr₂O₃ thin films was achieved for c -, r -, m - and a -plane oriented Al₂O₃ substrates. The orientation of both Cr₂O₃ and α -Ga₂O₃ thin film was the same as the respective substrate. For *ex situ* deposition of Ga₂O₃, XRD measurements indicate the presence of the χ -phase of Ga₂O₃, which is less dominant than the α -phase. No optimization was performed for the deposition process, but the results serve as a proof of concept that the deposition of phase-pure α -Ga₂O₃ – especially in the c - and r -orientation – is possible on Cr₂O₃ buffer layers.

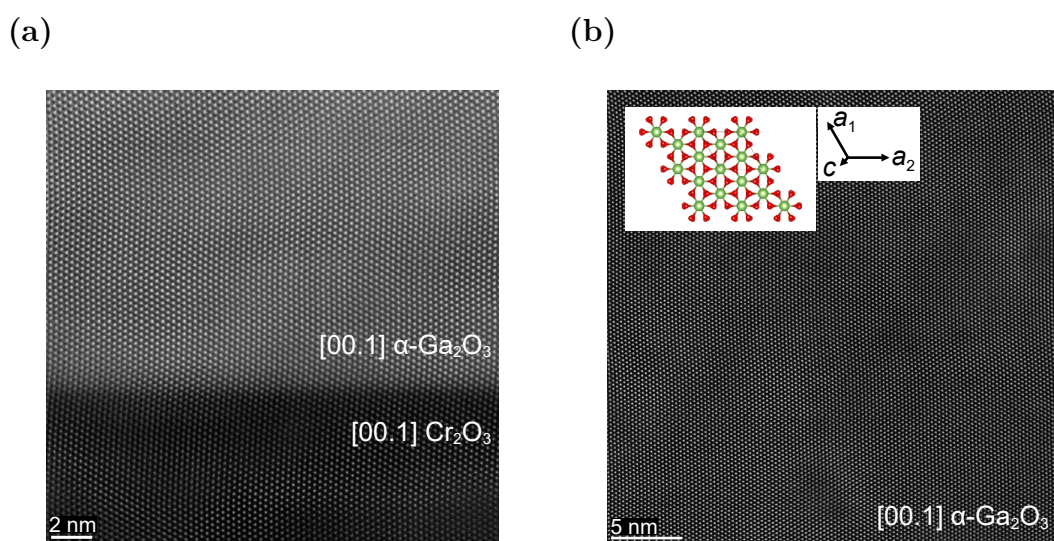


Figure 3.42: Images of the m -plane buffer layer structure: (a) HAADF image of the interface between Cr_2O_3 and $\alpha\text{-Ga}_2\text{O}_3$. (b) HAADF representative image of the $\alpha\text{-Ga}_2\text{O}_3$ layer. Courtesy of Dr. J. G. Fernandez. The image of the $\alpha\text{-Ga}_2\text{O}_3$ crystal structure was made with VESTA Ver. 3 [4].

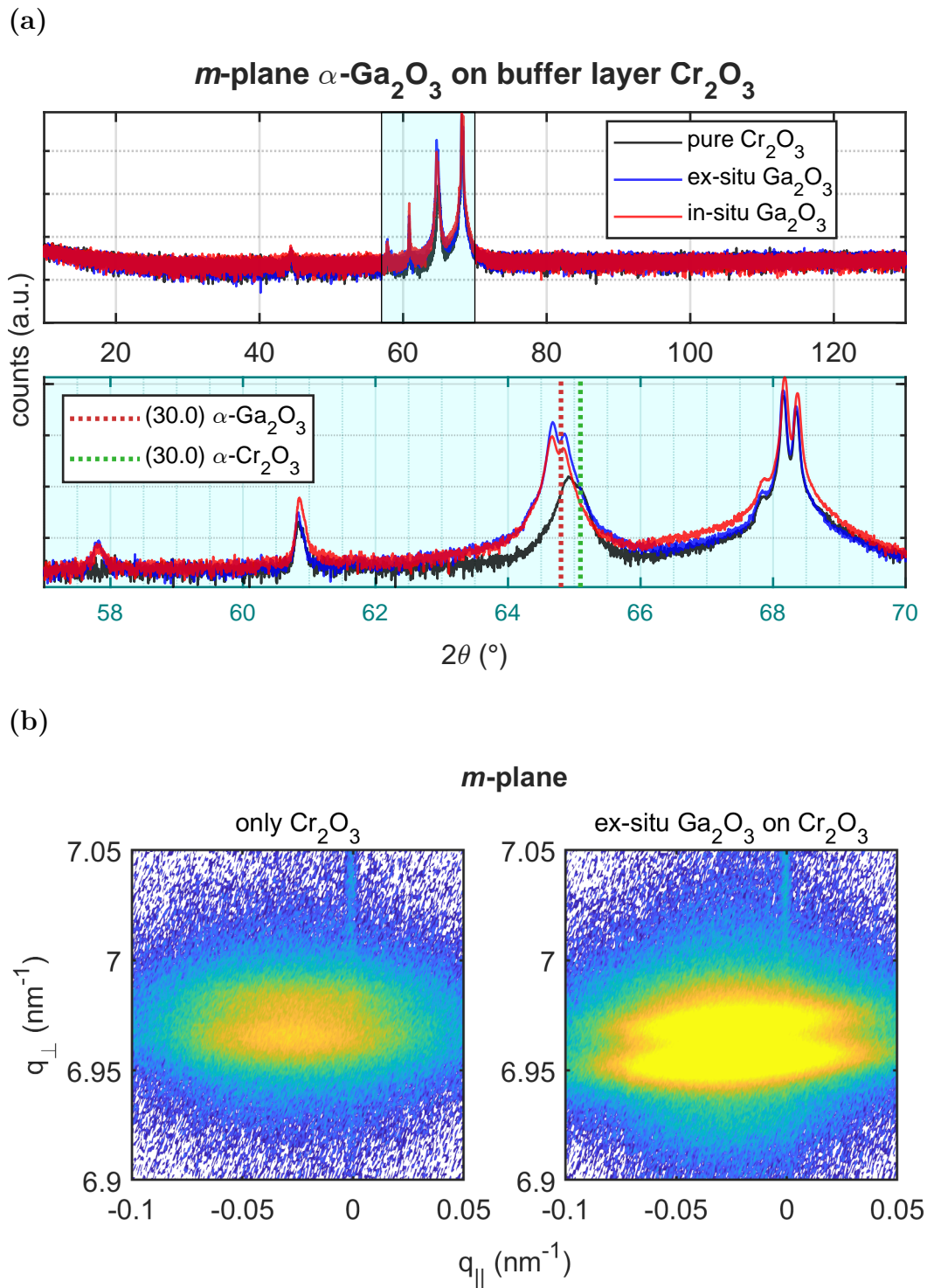


Figure 3.43: (a) $2\theta\text{-}\omega$ -patterns of the *m*-plane Cr_2O_3 reference sample (black), as well as the *ex situ* (blue) and *in situ* (red) buffer layer structures. The expected peak positions for the (30.0) reflection of Cr_2O_3 (green dotted) and $\alpha\text{-Ga}_2\text{O}_3$ (red dotted) are indicated. (b) RSM around the (30.0) reflection recorded before (left) and after (right) *ex situ* deposition of Ga_2O_3 on Cr_2O_3 .

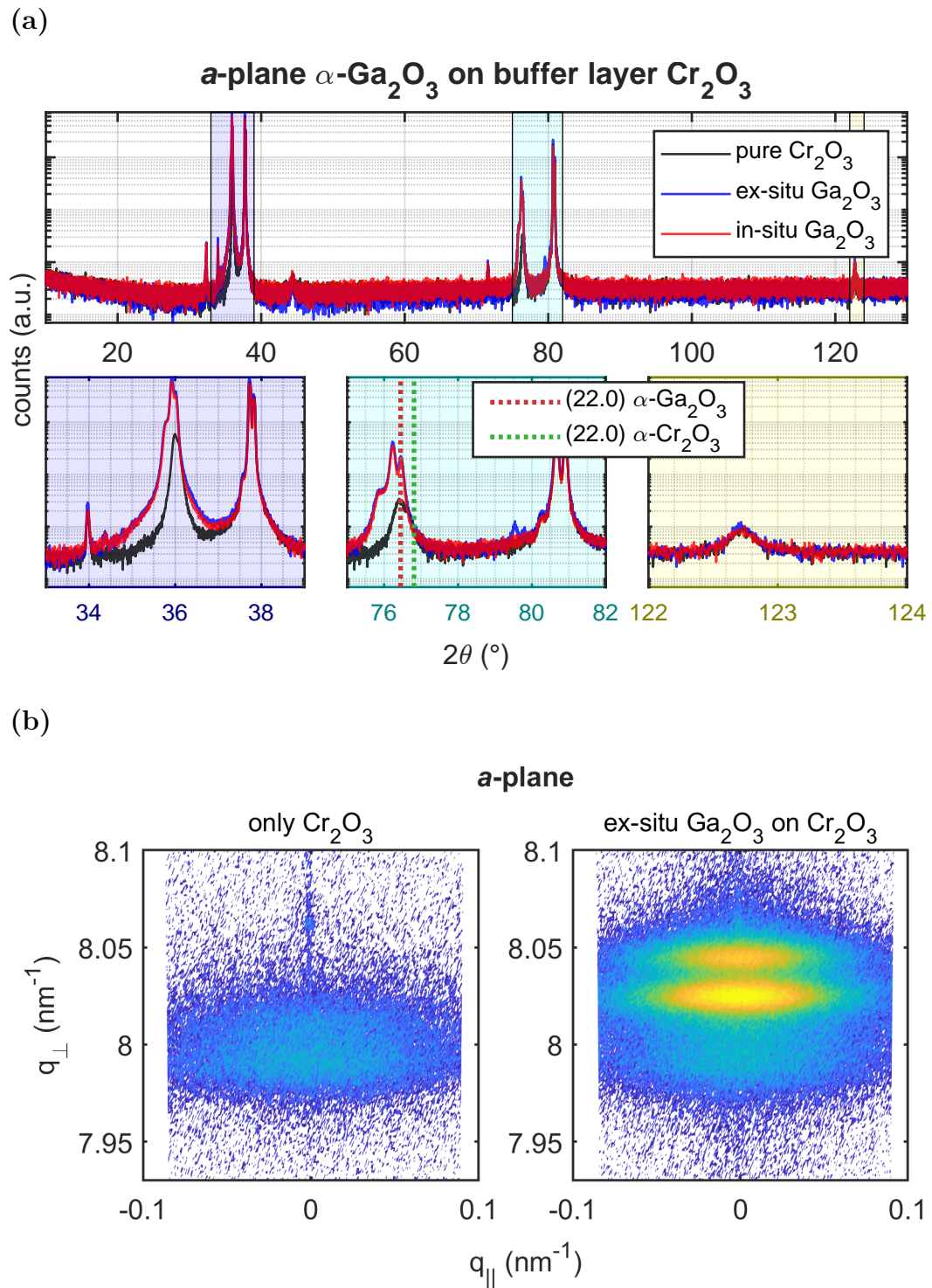
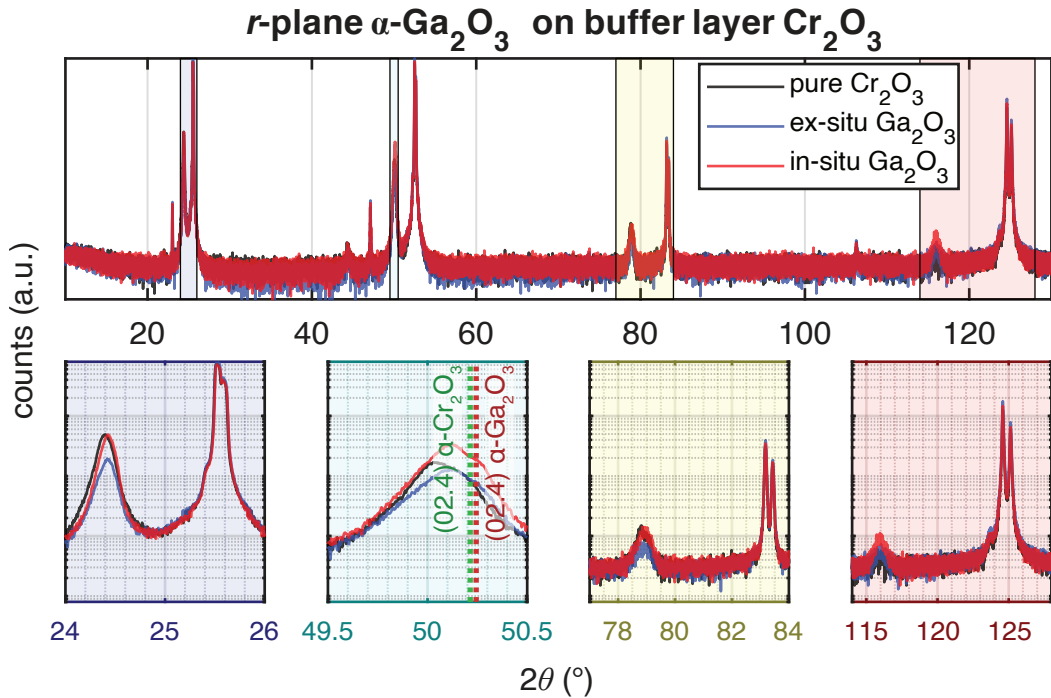


Figure 3.44: (a) $2\theta\text{-}\omega$ -patterns of the a -plane Cr_2O_3 reference sample (black), as well as the *ex situ* (blue) and *in situ* (red) buffer layer structures. The expected peak positions for the (22.0) reflection of Cr_2O_3 (green dotted) and $\alpha\text{-Ga}_2\text{O}_3$ (red dotted) are indicated. (b) RSM around the (22.0) reflection recorded before (left) and after (right) *ex situ* deposition of Ga_2O_3 on Cr_2O_3 .

(a)



(b)

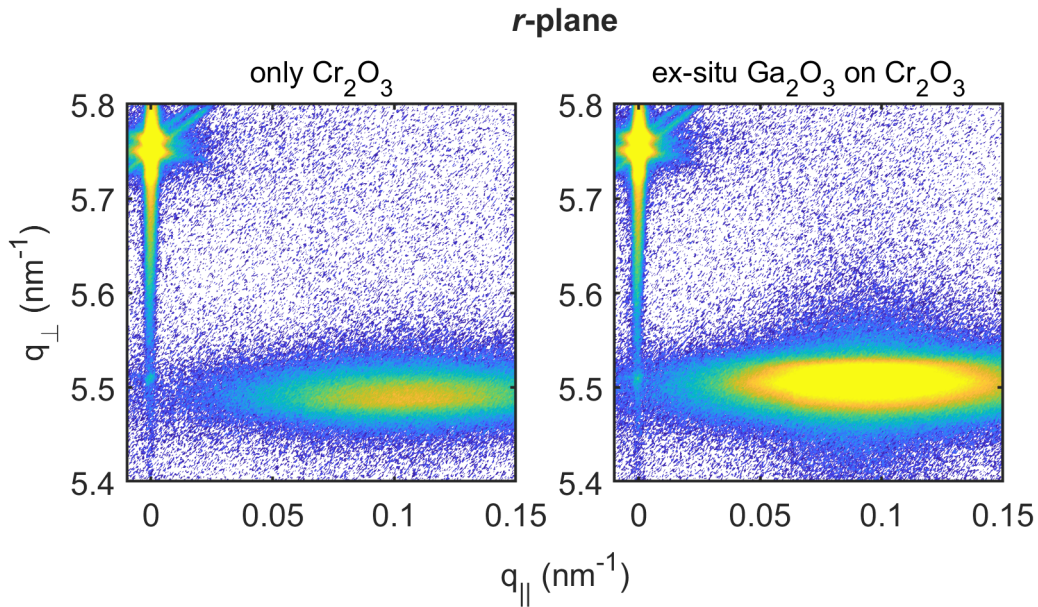


Figure 3.45: (a) $2\theta\text{-}\omega$ -patterns of the *r*-plane Cr_2O_3 reference sample (black), as well as the *ex situ* (blue) and *in situ* (red) buffer layer structures. The expected peak positions for the (02.4) reflection of Cr_2O_3 (green dotted) and $\alpha\text{-Ga}_2\text{O}_3$ (red dotted) are indicated. (b) RSM around the (02.4) reflection recorded before (left) and after (right) *ex situ* deposition of Ga_2O_3 on Cr_2O_3 .

Bibliography

- [1] S.I. Stepanov *et al.* “HVPE growth of corundum-structured α -Ga₂O₃ on sapphire substrates with α -Cr₂O₃ buffer layer”. In: *Materials Physics and Mechanics* 47 (2021), pp. 577–581. DOI: [10.18149/MMP.4742021_4](https://doi.org/10.18149/MMP.4742021_4).
- [2] Anubhav Jain *et al.* “Commentary: The Materials Project: A materials genome approach to accelerating materials innovation”. In: *APL Materials* 1.1 (2013), p. 011002. ISSN: 2166-532X. DOI: [10.1063/1.4812323](https://doi.org/10.1063/1.4812323).
- [3] Anna Hassa. “Epitaxy and Physical Properties of Group-III Sesquioxide Alloys”. PhD thesis. Leipzig University, 2021.
- [4] Koichi Momma and Fujio Izumi. “VESTA 3 for three-dimensional visualization of crystal, volumetric and morphology data”. In: *Journal of Applied Crystallography* 44.6 (2011), pp. 1272–1276. ISSN: 0021-8898. DOI: [10.1107/S0021889811038970](https://doi.org/10.1107/S0021889811038970).